Zheng *et al.*
Chinese Journal of Mechanical Engineering (2022) 35:137
https://doi.org/10.1186/s10033-022-00810-4

Chinese Journal of Mechanical Engineering

ORIGINAL ARTICLE

Open Access

Corrosion Resistance and Tribological Properties of Laser Cladding Layer of H13 Die Steel Strengthened by Ultrasonic Rolling

Kaikui Zheng[1,2*], Youxi Lin[1], Jianguo Cai[3] and Chengqian Lei[1]

Abstract

Laser cladding is a new surface repair method that can improve the wear and corrosion resistance of substrate surfaces. However, the cladding layer typically exhibits a rough surface, high hardness and large residual tensile stress, and thus requires further machining and finishing. Ultrasonic rolling (U-rolling) is a highly efficient finishing and strengthening process that combines ultrasonic technology with traditional rolling (T-rolling). In this study, an iron-based alloy was coated onto the surface of H13 die steel using laser cladding, and the surface of the cladding layer was polished using U-rolling. The effects of U-rolling on the surface quality, corrosion resistance and friction and wear properties of the laser-cladding layer were investigated and compared with those obtained by T-rolling. The surface roughness of the U-rolled sample was only 1/4 that of the T-rolled sample. The hardness and residual compressive stress of the laser cladding layer after U-rolling were higher than those after T-rolling. Similarly, the surface corrosion resistance of the laser cladding layer after U-rolling was higher than that after T-rolling. U-rolling changed the surface roughness, grain size, and residual stress of the material and thus affected the corrosion resistance of the laser cladding layer. The friction coefficient and wear rate of the U-rolled surface of the cladding layer were lower than those of the T-rolled surface. In addition, the tribological properties of the cladding layer were found to be related to the rolling direction. When the friction direction of the sample was the same as the rolling direction, its friction and wear performance were higher than those when the two directions were perpendicular.

Keywords: Laser cladding, Ultrasonic rolling, Surface quality, Corrosion resistance, Tribological properties

1 Introduction

Molds are importanial products, such as automobiles, household appliances, and aerospace components, and the rapid development of such industries demands good quality and long service life of molds [1]. The failure of die wear, corrosion and fatigue fracture often starts at the surface or is caused by surface factors [2–4]. With the development of molds for achieving diversification, refinement, and complexity in the final products, higher requirements have been proposed for the repair of failed molds, which is a considerable challenge for traditional mold repair processes [5]. The surfacing welding is simple and has a wide range of applications; however, it has a high dilution rate and produces a large heat-affected zone on the substrate [6]. Thermal spraying equipment is simple and easy to operate, but the bonding between the repair layer and substrate is weak [7]. Laser cladding, as a new surface treatment technology, has several advantages, such as a small heat-affected zone, strong bonding with the matrix, large cladding layer thickness, fine structure, and excellent performance [8, 9]. The characteristics of the abovementioned mold repair methods are listed in Table 1.

In recent years, laser cladding technology has rapidly developed and has been widely used in automobiles,

*Correspondence: kuikui@fzu.edu.cn

[1] School of Mechanical Engineering and Automation, Fuzhou University, Fuzhou 350116, China
Full list of author information is available at the end of the article

Table 1 Characteristics of common mold repair methods

Repair method	Surfacing weld	Thermal spraying	Laser cladding
Heat source	Arc, plasma arc, etc	Flame, plasma arc, etc	Laser
Heat affected zone	Large	Small	Small
Dilution ratio (%)	2–60	1–5	1–11
Cladding speed (kg/h)	0.5–6.8	1–10	13–16
Bonding strength with matrix	Metallurgical bonding	Mechanical bonding	Metallurgical bonding

aerospace engineering, mold manufacturing, and repair [10, 11]. Xu et al. [12, 13] realized the remanufacturing of shaft and tooth parts of heavy vehicles and aluminum alloy cylinder heads of automobile engines using laser cladding. Zhao et al. [14] used FeCr alloy powder to prepare a repair layer on a preset defect-containing KMN steel matrix via laser cladding. The hardness of the repair layer was 1.8 times that of the matrix material, and the wear resistance and corrosion resistance were significantly improved. Pham et al. [15] used the preset powder method for cladding Co50-and TiC/Co-based powders on the surface of H13 steel. The hardness values of the two alloy powder cladding layers were significantly higher than that of the matrix. H13 steel has good strength and toughness and is a hot-work die steel that is widely used in industry. Kattire et al. [16] prepared a CPM 9V powder coating on the surface of H13 die steel via synchronous powder feeding. The obtained cladding layer exhibited high hardness and wear resistance. Huang et al. [17] prepared a $NiCr/Cr_3C_2$ composite cladding layer on the surface of H13 steel via synchronous powder feeding; the prepared cladding layer showed high wear resistance and an average friction coefficient smaller than that of the substrate. Cong et al. [18] deposited an iron-based alloy cladding layer on the surface of H13 die steel via synchronous powder feeding and observed that the laser cladding could repair most of the thermal cracks on the die surface, and the thermal fatigue resistance was significantly improved compared to that of the matrix. Laser cladding repair produces only a small thermal deformation and metallurgical combination; therefore, it is highly popular for hot-work die repair. However, the surface of the cladding layer is uneven with distinct valleys and peaks, and the unmelted powder is easily bonded to the cladding surface. The residual tensile stress of the cladding layer is very large, which can render the repair structure uneven; therefore, further machining and finishing are required. Common finishing methods include grinding [19], polishing [20], and rolling [21]. Because the hardness of the laser cladding layer is often high, grinding and polishing are commonly used. However, they have low efficiency and require high energy consumption.

Rolling is an economical and efficient finishing and strengthening process that can change surface quality factors such as surface roughness, microhardness, residual stress, and microstructure, thereby enhancing the resistance of the repair layer to corosion, friction, wear, and fatigue [22–24]. Zhang et al. [25] processed a Cr/Ni cladding layer using a composite turning rolling process, which eliminated turning tool marks via low-plastic rolling, and improved the corrosion resistance of the cladding layer. However, surface hardening reduces surface corrosion resistance because of the small amplitude and shallow action depth of the residual compressive stress produced by traditional rolling (T-rolling), which limits its strengthening effect [26]. The large static pressure required during T-rolling easily causes scratches, tears, and adverse residual shear stress on the machined surface, making it unsuitable for thin-walled or slender shafts. Liu et al. [27] reported that when the rolling pressure increases by a certain value, part of the surface peels off, decreasing the surface quality. In ultrasonic rolling (U-rolling), ultrasonic machining is applied to T-rolling, and its strengthening effect is better than that of T-rolling [28]. Zhang et al. [29] demonstrated that owing to the joint action of hardness and residual compressive stress, the wear resistance after rolling was improved, and the friction coefficient and wear rate decreased to 10% and 25%, respectively. Qin et al. [30] performed U-rolling on AISI 52100 steel to produce nanostructures on the surface of the material, thereby improving the wear resistance and pitting corrosion resistance of the material.

To date, U-rolling of the laser cladding layer has rarely been investigated. In this study, U-rolling technology was used to polish and strengthen the laser cladding layer of H13 die steel, and the effects of U-rolling on the corrosion resistance and tribological properties of the cladding layer were studied and compared with those of T-rolling. The obtained results provide an experimental basis and technical guidance for the implementation of U-rolling in the finishing and strengthening of laser

Table 2 Chemical compositions of H13 die steel (mass fraction, %)

Element	C	Mn	Si	S	P	Ni	Cr	V	Mo	Cu	Fe
Content	0.393	0.41	1.05	0.003	0.013	0.16	5.29	0.98	1.31	0.09	Balance

Table 3 Chemical composition of iron-based alloy powder (mass fraction, %)

Element	P	S	Ni	Cr	Fe
Content	0.013	0.005	2.4	18.71	Balance

cladding layers of die steel and extend the applications of U-rolling in die manufacturing and repair.

2 Experimental Procedures

2.1 Preparation of Laser Cladding Layer

2.1.1 Substrate

The material used as the substrate was H13 die steel: it was processed into a cladding substrate with dimensions of 100 mm × 100 mm × 20 mm via wire cutting. The chemical composition of the substrate is presented in Table 2.

2.1.2 Alloy Powder

The H13 die steel was laser-cladded with an iron-based alloy powder, whose chemical composition and physical properties are listed in Tables 3 and 4, respectively.

2.1.3 Preparation of Laser Cladding Layer

Before laser cladding, the oxide film and rust layer of the H13 matrix were removed by sandpaper, followed by ultrasonic cleaning in alcohol to remove oil stains; the iron-based alloy powder was dried. A schematic of laser cladding is shown in Figure 1. A compact fiber laser (nLight, United States) with a maximum output power of 2000 W was used for laser cladding. The laser cladding layer was prepared using a synchronous powder feeding method. The cladding head was driven by a machine arm, and a special powder feeder was configured simultaneously. The cladding head was mainly composed of a laser beam cavity, carrier gas powder cavity, and inner protective gas cavity. The powder feeding pipe was evenly and symmetrically positioned in the cladding head, and the alloy powder was fed coaxially and collected at the nozzle to improve its utilization rate. N_2 was used as the powder feeding gas, as well as a shielding gas to prevent the reaction between air and the melting pool. The laser beam was focused in the Z-direction through the focusing lens; the alloy powder absorbed a fraction of the beam energy, and the remaining beam was transmitted to the substrate surface. Finally, the substrate surface material and the alloy powder were fused to form a cladding layer. The laser cladding parameters are listed in Table 5, and the laser cladding layer is shown in Figure 2.

2.2 Milling of Laser Cladding Layer

The KMC600U five-axis machining center (Figure 3) was used to mill the laser cladding layer, which could not be milled using ordinary cemented carbide because of rapid tool wear and even tool collapse. To ensure stable cutting of the laser cladding layer, an integral boron nitride blade (SNMN20412) was used as the milling tool. The milling process parameters were as follows: milling speed of 450

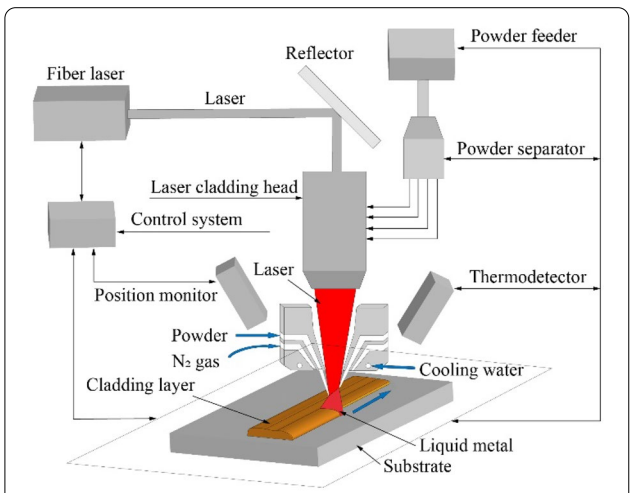

Figure 1 Schematic of laser cladding

Table 4 Physical properties of iron-based powder

Apparent density(g/cm^3)	Fluidity	Particle size distribution(%)					
		≤ 53	53–71	71–106	106–150	150–180	180–212
3.62	22.1s/50g	1.39	17.39	43.20	32.75	5.06	0.21

Table 5 Laser cladding parameters

Parameter	Laser output power (W)	Laser wavelength(nm)	Scanning rate(mm/s)	Defocus amount(mm)	Shielding gas pressure(MPa)	Gas carrying capacity(L/min)
Value	1100	1064	5	14	0.1	12

Figure 2 Laser cladding layer on H13 die steel

Figure 3 Processing equipment

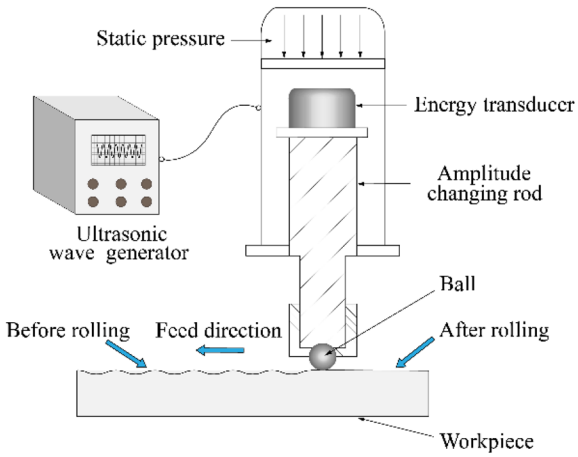

Figure 4 Schematic of ultrasonic rolling

r/min, feed speed of 80 mm/min, and milling depth of 0.12 mm.

2.3 Rolling of Cladding Layer

HK30G U-rolling equipment was installed on a five-axis machining center (Figure 3). A schematic of U-rolling is shown in Figure 4. A ball with a radius of 7 mm was installed at the face of the output end of the ultrasonic horn. During the installation, the new ball rolled flexibly in the tool seat without blocking. The axial displacement of the ball was adjusted by tightening the set screw to ensure that the displacement was less than 0.03–0.05 mm. Finally, the vertical machining center program was started to bring the actuator ball into contact with the workpiece, and the cladding layer was rolled on the surface of the H13 die steel. The U-rolling process parameters were as follows: current of 1.1 A, pressing distance of 0.1 mm, rolling rate of 1800 mm/s, step distance of 0.03 mm, and static pressure of 0.55 MPa. T-rolling was performed using the same equipment and process parameters as U-rolling but without turning on the ultrasonic source.

2.4 Surface Quality Characterization

The surface roughness of the workpiece was characterized using a TR200 surface roughness instrument. Before testing the surface roughness, the workpiece was ultrasonically cleaned.

$$Ra = \frac{1}{l}\int_0^l |Z(x)|\mathrm{d}x, \tag{1}$$

where, Ra, the arithmetic mean of the absolute value of the ordinate $Z(x)$ within sample length l, was selected as the evaluation index of the surface roughness.

An HR-150A Rockwell hardness tester was used to measure the surface hardness. For each sample, the

surface hardness values at five selected test points were evaluated, and the arithmetic mean was used as the surface hardness of the sample. The microhardness of the laser cladding layer along the depth direction before and after U-rolling was measured using an MVC-1000D1 microhardness tester.

The residual stress on the workpiece surface was measured using a PROTO iXRD residual stress testing system with a CR target X-ray tube, tube voltage of 20 kV, and tube current of 4 mA. The material properties of the cladding layer were set as follows: (211) diffraction crystal plane, body-centered cubic symmetrical profile, Bragg angle (2θ) of 156.41°, Poisson's ratio of 0.28, and an elastic modulus of 213.64 GPa. Diffraction peaks were determined using Gaussian fitting.

2.5 Electrochemical Performance Test

The corrosion resistance of the surface of the cladding layer was tested on a Gamry interface 1010E electrochemical workstation, and polarization and AC impedance spectra were obtained. The electrochemical samples were processed into 10 mm × 10 mm × 12 mm cuboids by wire cutting, ground with 80–3000# sandpaper, and their four sides were mirror polished. These samples were then encapsulated in epoxy resin, and the laser cladding layer was used as the working surface, which was then polished again. The electrochemical tests were performed using a three-electrode system: a Pt electrode as the counter electrode, laser cladding sample as the working electrode, saturated calomel electrode as the reference electrode, and 3.5% NaCl as the corrosion solution. The morphology of the corroded sample surface was characterized using scanning electron microscopy (SEM; Quanta 250 tungsten filament scanning electron microscope).

2.6 Friction and Wear Performance Test

An MMS-2A microcomputer-controlled friction testing machine was used to test the ring–block friction and wear properties of the laser cladding layer before and after U-rolling. A schematic of the test setup is shown in Figure 5. The sample size was 30 mm × 8 mm × 6 mm; the dual part was a GCr15 steel ring with an inner diameter of 16 mm, an outer diameter of 40 mm, and hardness of HRC60. A test load of 200 N, test speed of 2000 r/min, and test time of 60 min for continuous friction were used, and the average value of the friction coefficient in the stable wear stage was selected as the friction coefficient. The wear surface morphology of the samples was analyzed using SEM.

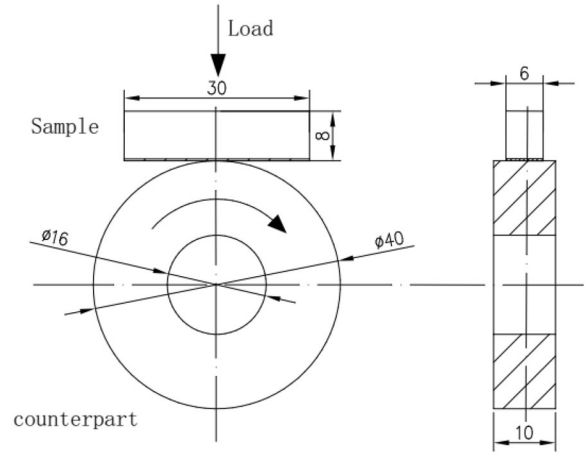

Figure 5 Schematic of ring–block friction and wear test

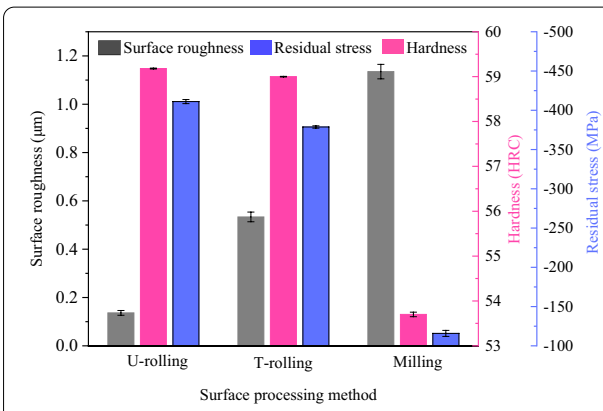

Figure 6 Effect of U-rolling on surface quality of cladding layer

3 Results and Discussion

3.1 Effect of U-rolling on Surface Quality of Laser Cladding Layer

The laser cladding surface of the H13 die steel was processed by both U-rolling and T-rolling, and the initial roughness was 1.135 μm. The effects of U-rolling, T-rolling, and milling on the surface roughness, hardness, and residual stress of the laser cladding layer are shown in Figure 6.

As shown in Figure 6, U-rolling or T-rolling reduced the surface roughness of the cladding layer and improved the hardness and residual compressive stress. The surface roughness of the cladding layer processed by U-rolling is 0.1364 μm, which is much lower than that obtained by T-rolling (0.533 μm), that is, the surface roughness produced by U-rolling is only 1/4 of that produced by T-rolling. The hardness and residual compressive stress of the laser cladding layer after U-rolling are higher than those after T-rolling. U-rolling technology uses a combination of ultrasonic impact energy and static load rolling to

strengthen the surface of metal parts. In U-rolling, a certain range of ultrasonic frequencies is applied along the normal direction of the workpiece surface through the machining working head to produce mechanical vibrations. Under certain feeding conditions, the working head transmits static pressure and ultrasonic impact vibration to the surface of the rotating mechanical parts, resulting in extrusion and large elastic–plastic deformations in the metal-based materials. After machining, a certain elastic recovery occurs on the workpiece surface, and the resulting plastic flow fills the "valley" on the workpiece surface with a "peak" or partially, thereby reducing the surface roughness of the part to the nanoscale. During T-rolling, only static pressure (no dynamic pressure) is applied; therefore, the surface hardening effect is not as high as that of U-rolling. The amplitude of the residual compressive stress produced by T-rolling is small, and the affected depth is low, resulting in a limited strengthening effect [31, 32].

3.2 Effect of U-rolling on Corrosion Resistance of Laser Cladding Layer

Electrochemical tests were performed on the surface of the H13 die steel laser cladding layer after milling, T-rolling, and U-rolling. Figure 7 shows the polarization curves of the laser-cladding layers processed using different electrochemical tests. The self-corrosion potential and corrosion current data of the samples were obtained using the Tafel extrapolation method, and the corresponding results are listed in Table 6. As shown in Figure 7, the polarization curves of the three surface-processed samples have similar shapes, indicating that their electrochemical reactions in the corrosion

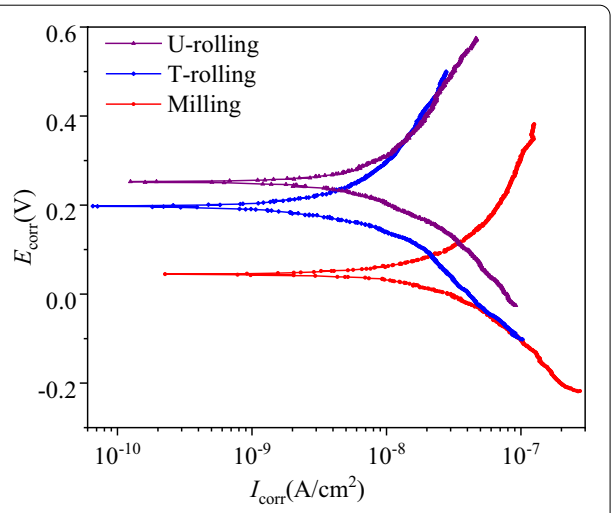

Figure 7 Potentiodynamic polarization curves for different samples

Table 6 Self-corrosion potential and self-corrosion current density of samples

Samples	E_{corr} (V)	I_{corr} (A•cm^{-2})
U-rolling	0.2531	9.8528×10^{-9}
T-rolling	0.1965	6.6929×10^{-9}
Milling	0.0490	2.2356×10^{-8}

solution are similar. Figure 7 and Table 6 show that the self-corrosion potential of the U-rolled sample is 0.2531 V, which is higher than that of the T-rolled sample (0.1965 V), whereas the self-corrosion potential of the latter is higher than that of the milled laser cladding surface (0.0490 V). The self-corrosion current densities of U-rolled and T-rolled samples are of the same order of magnitude: one order of magnitude lower than that of the milled laser cladding surface. Self-corrosion potential is the potential at which corrosion can occur. A high corrosion potential impedes the corrosion reaction, thereby reducing the possibility of corrosion. Evidently, the proneness to corrosion of the milled cladding surface is the highest, followed by that of the T-rolled sample, and then the U-rolled sample. According to Faraday's law, the corrosion rate of a metal is directly proportional to the corrosion current density I_{corr} [33]; therefore, the corrosion rate of the milled surface is higher than that of the U-rolled and T-rolled surfaces. Furthermore, there is a negligible difference between the corrosion rates induced by T-rolling and U-rolling.

No clear passivation zone is observed in the polarization curves (Figure 7) of the three samples. According to the electrochemical reaction process, the polarization curve can be divided into cathode and anode polarization curve areas. The cladding layer mainly exhibits the cathodic oxygen reduction in 3.5% NaCl electrolyte, which consumes the electrons produced by the anodic oxidation reaction. The cathodic reduction reaction can be expressed as Eq. (2).

$$O^2 + 2H_2O + 4e \rightarrow 4OH^-. \quad (2)$$

In the anodic polarization zone, the anodic dissolution reaction of Fe is completely controlled by activation, and the anodic oxidation reaction may be expressed as

$$Fe \rightarrow Fe^{2+} + 2e. \quad (3)$$

The total chemical reaction is

$$2Fe + O_2 + 2H_2O \rightarrow 2Fe(OH)_2. \quad (4)$$

In the presence of additional oxygen, ferrous hydroxide easily reacts with the dissolved oxygen, and it is finally

converted into water and the corrosion product, iron oxide. The reaction is shown as

$$6Fe(OH)_2 + O_2 \rightarrow 2Fe_3O_4 + 6H_2O. \quad (5)$$

According to Eq. (5), the surface of the material forms an oxide film through the oxidation reaction. Cl^- easily penetrates the pores or defects of the film through diffusion and reacts with the metal to form active dissolution products. Thus, Cl^- changes the electronic and ionic conductivities of the oxide film, thereby damaging its protective effect.

To further evaluate the electrochemical characteristics of laser cladding layer before and after U-rolling and T-rolling in 3.5% NaCl, the AC impedance spectra (Nyquist curves) of the samples were obtained, as shown in Figure 8. The three Nyquist curves in Figure 8 have similar shapes, indicating that the three processed surfaces exhibit similar AC impedance spectral characteristics. Considering the arc curvature radius, the samples follow the order of U-rolled > T-rolled > milled surface. A larger curve radius of the capacitive arc indicates higher corrosion resistance of the material. Notably, the corrosion resistance of the U-rolled sample is the best, followed by that of the T-rolled sample, whereas that of the milled laser cladding surface is the worst.

The corrosion resistance of the samples processed using different methods was further characterized using Gamry Echem Analyst software: the measured AC impedance spectra were fitted using the equivalent circuit method, and the Bode curves of the samples were obtained, as shown in Figure 9. As shown in Figure 9(a), the order of amplitude in the medium- and low-frequency regions (10^{-2} < Frequency < 1) is as follows: U-rolled > T-rolled > milled surface. This amplitude

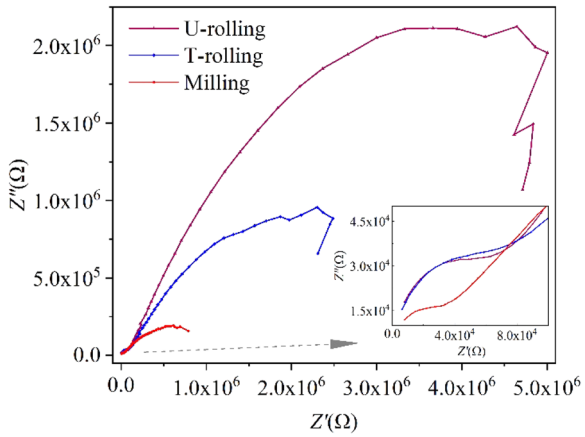

Figure 8 Electrochemical impedance spectroscopy for different samples

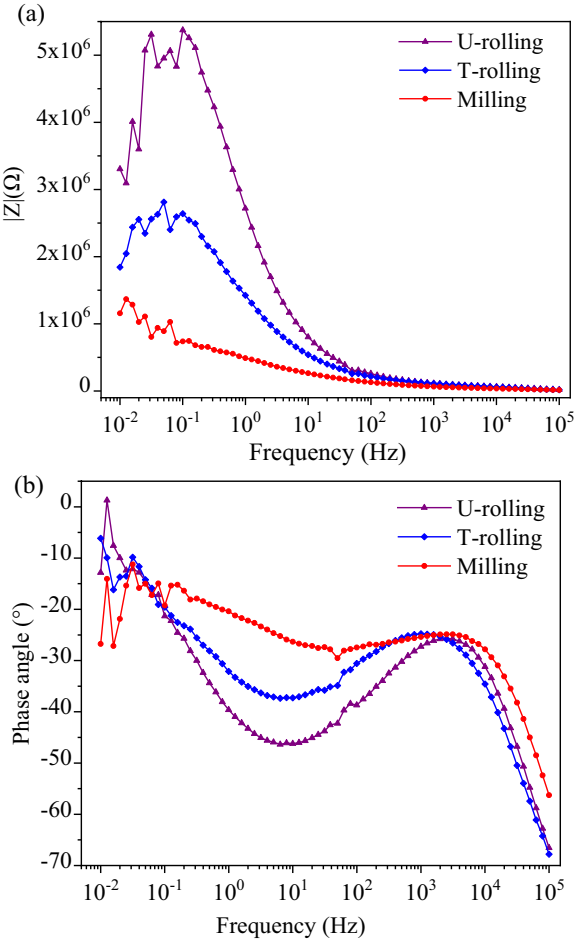

Figure 9 Bode curve of samples: (**a**) Frequency–amplitude, (**b**) Frequency–phase angle

reflects the impedance value of the metal surface, indicating that a larger amplitude corresponds to a higher impedance value, that is, higher corrosion resistance of the material. The corrosion resistance of the U-rolled sample is higher than that of the T-rolled one, and that of the milled laser cladding sample is the worst, which is consistent with the Nyquist curve. The high-frequency region (frequency > 10^4 Hz) characterizes the solution impedance. The three curves in Figure 9 basically coincide in the high-frequency region, and the impedance value is ~ 10 kΩ, indicating that the impedances of the laser cladding layer in the high-frequency region before and after rolling are approximately equal. In the Bode phase diagram (Figure 9(b)), all the samples exhibit two peaks, indicating that they have two time constants and are double-capacitor layer structures. Based on the aforementioned results, combined with the test and analysis results of the polarization curves and electrochemical impedance spectroscopy, it can be concluded that the

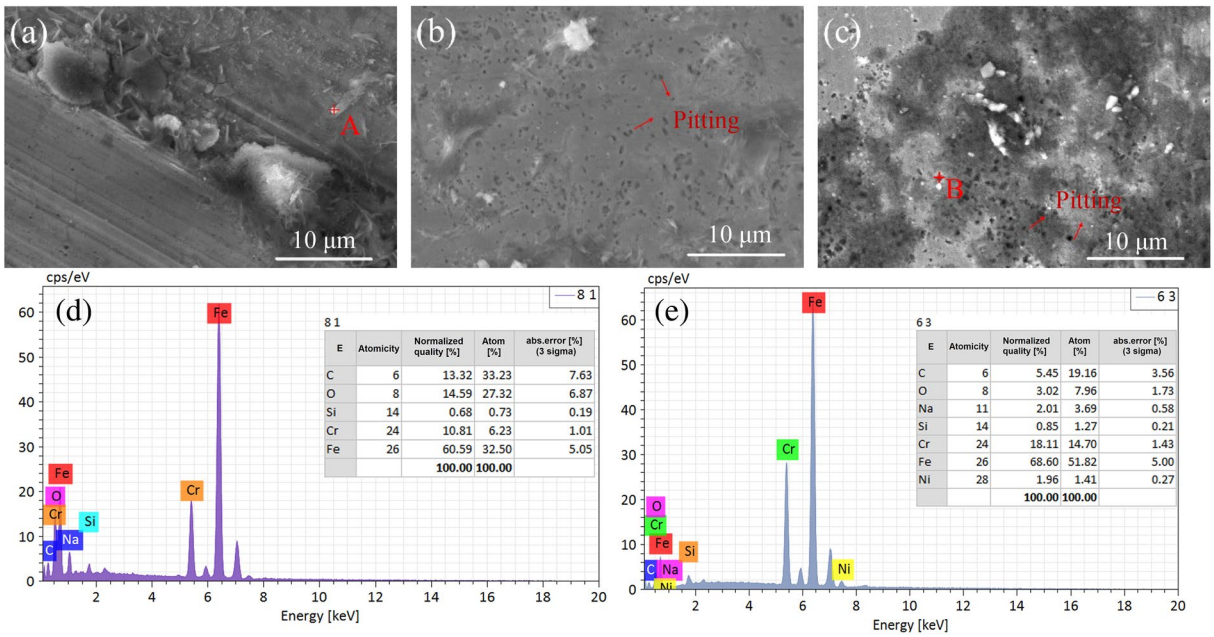

Figure 10 Corrosion morphology of the samples: (**a**) Milled, (**b**) U-rolled, (**c**) T-rolled, Energy spectra at positions (**d**) A and (**e**) B

surface corrosion resistance of the laser cladding layer follows the order of U-rolled > T-rolled > milled surface.

To further analyze the effects of different surface processing methods on the surface corrosion resistance of the laser cladding layer, the corrosion morphologies of the samples were observed and analyzed using SEM and energy-dispersive X-ray spectroscopy, and the results are shown in Figure 10. Evidently, the surface of the laser cladding layer after U-rolling exhibits the weakest corrosion pitting (Figure 10(b)), followed by T-rolling (Figure 10(c)), whereas the milled surface shows the strongest corrosion pitting with a large amount of corrosion products accumulated (Figure 10(a)).

As shown in Figure 10(d) and (e), the corrosion products are mainly composed of Fe, Cr, and O, indicating that the corrosion products are mainly comprised by chromium oxide and iron oxide or hydride; a small amount of Na could originate from the residual electrolyte. The laser cladding layer, before and after rolling, contains more corrosion-resistant elements, such as Cr and Ni. Cr forms Cr_2O_3, which protects the metal surface and improves its corrosion resistance. A higher surface roughness implies that a large amount of corrosive liquid or gas is likely to penetrate the inner metal layer through the microvalleys on the surface, resulting in surface corrosion. Grain refinement [34] has two effects on corrosion resistance: first, it reduces corrosion resistance in the activated zone because of an increase in the grain boundaries and the accumulation of crystal defects (high-density dislocations and slip bands); second, the corrosion resistance is improved after metal passivation. In addition, the residual compressive stress formed on the surface can prevent further propagation of cracks and improve the corrosion resistance of the surface. The residual compressive stress increases the surface atomic density of the laser cladding material, reduces surface activity, and improves corrosion resistance. In summary, the effects of U-rolling on the corrosion resistance of the laser cladding layer originate from the combined changes in the chemical and physical properties (surface roughness, grain refinement, and residual compressive stress) of the surface of the material.

3.3 Effect of U-rolling on Friction and Wear Properties of Laser Cladding Layer

Ref. [35] showed that when the friction direction is the same as the rolling direction, the friction coefficient and wear volume of the materials are lower than when the two directions are perpendicular. Therefore, the T-rolled sample with both friction and rolling in the same direction was used as a comparison for the U-rolled sample. The friction and wear properties of the surface of the H13 die steel laser cladding layer after milling, T-rolling, and U-rolling were also evaluated. The sample with the friction direction perpendicular to the rolling direction was labeled U-rolling-V, while that with both friction and rolling in the same direction was named U-rolling-H. The results are shown in Figure 11. The friction coefficient

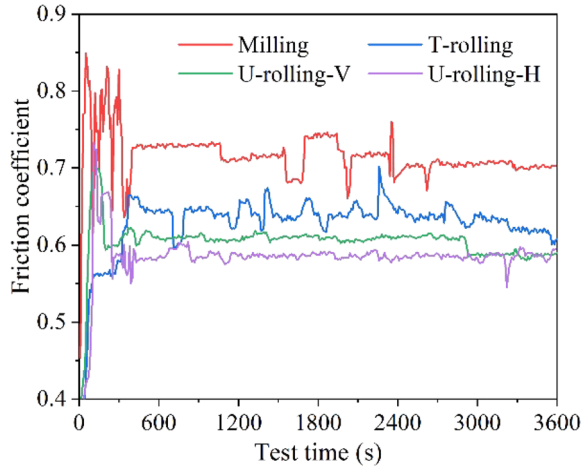

Figure 11 Friction coefficient

of the sample is the average value of the friction coefficients in the stable wear stage (test time of 1200–2400 s). As shown in Figure 11, the friction coefficient of the laser cladding layer after U-rolling is the smallest, followed by that of the T-rolled sample. Furthermore, the friction coefficient of the non-rolling sample is the largest. The friction coefficient of the U-rolling-H sample is 0.586, which is lower than that of the U-rolling-V sample.

White-light interferometry was used to scan and measure the grinding pit profile of the samples, as well as the cross-sectional grinding pit profile curves of the samples before and after the friction and wear tests (Figure 12(a)). The wear volume and wear rate of the samples (Figure 12(b)) were calculated according to Eqs. (6) and (7) [36]. The dimensions of the grinding pits of the samples are listed in Table 7.

$$\Delta V = 14bh/3, \tag{6}$$

$$W = \Delta V/(\pi \cdot 2r \cdot n \cdot P), \tag{7}$$

where ΔV is the wear volume, b is the wear mark width, h is the wear mark depth, W is the wear rate, r is the outer diameter of the counterpart, n is the number of revolutions, and P is the load.

As shown in Figure 12 and Table 7, the width, depth, wear volume, and wear rate of the U-rolled sample are lower than those of the T-rolled sample, whereas the wear resistance of the milled surface is the worst. Moreover, the dimensions of the wear pits in different wear directions on the U-rolled samples are also different. The wear resistance of samples with the same friction and rolling directions is higher than that when the two directions are perpendicular.

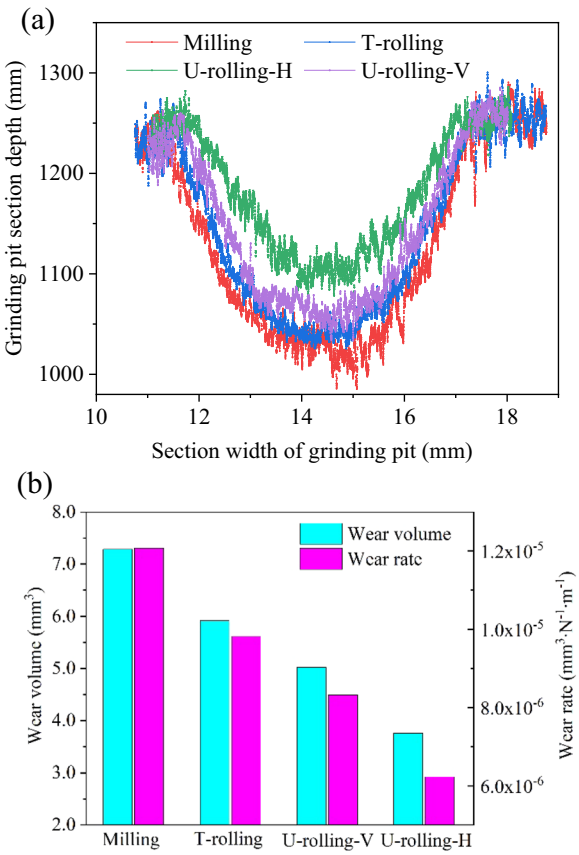

Figure 12 Wear properties of samples: (**a**) Grinding pit profile, (**b**) Wear volume and wear rate

To further analyze the effects of different surface processing methods on the surface wear characteristics of the laser cladding layer, the wear morphologies of the samples were analyzed by SEM, and the corresponding results are shown in Figure 13. As shown in Figure 13(a), during the friction between the microconvex body on the surface of the cladding layer and the dual part, the temperature in the contact area increased sharply, and the microconvex body softened and adhered. With increasing friction, the adhesive area expanded until attaining a certain thickness, at which the adhesive point

Table 7 Grinding pit size of laser cladding layer before and after rolling

Samples	b(mm)	h(μm)	ΔV(mm^3)	W(mm^3·N^{-1}·m^{-1})
Milling	6.229	250.594	7.285	1.208×10^{-8}
T-rolling	5.782	219.567	5.925	9.823×10^{-9}
U-rolling-V	5.572	193.030	5.020	8.323×10^{-9}
U-rolling-H	5.026	160.260	3.759	6.232×10^{-9}

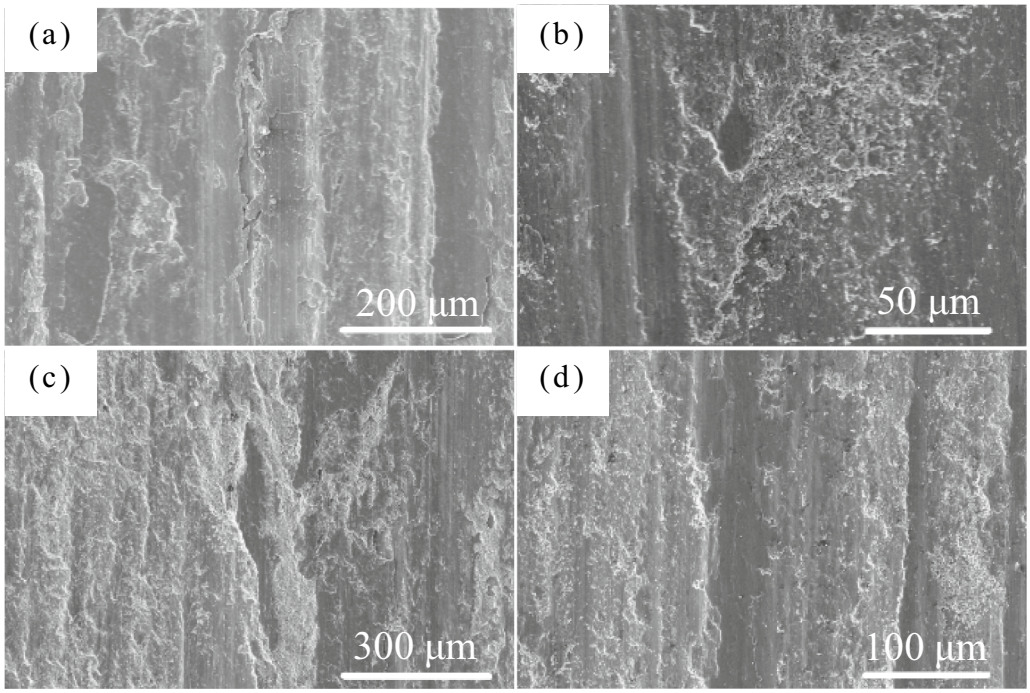

Figure 13 Wear properties of samples: (**a**) Milled, (**b**) T-rolled, (**c**) U-rolling-V, (**d**) U-rolling-H

was sheared and damaged under frictional shear stress, resulting in material wear. It can be observed that after milling, adhesive wear mainly occurs. In addition, some slight scratches can be observed on the worn surface of the sample because of the repeated rolling of the fallen adhesive layer on the surface on which friction is acting. This results in the formation of hard particles, causing wear of third-body abrasive particles and plow marks on the surface. Figure 13(b) indicates that the surface wear after T-rolling is mainly adhesive wear; however, some plow marks can be observed on the surface. Therefore, the T-rolled surface mainly exhibits adhesive wear accompanied by abrasive wear. As shown in Figure 13(c) and (d), the wear morphology of the surface treated by U-rolling contains a large number of plow marks and exhibits less adhesion than the T-rolled surface. Thus, primarily abrasive and adhesion wear of the surface occurred, resulting in higher wear of the U-rolling-H surface compared to the U-rolling-V surface.

The wear form of a material surface is closely related to its hardness. Low hardness results in adhesive wear, whereas high hardness causes abrasive wear. According to the Archard theory, increasing the surface hardness of a material can effectively enhance its wear resistance. Furthermore, an increase in the hardness of the material can increase its deformation resistance, reduce the adhesion between the material surface and friction pair, and reduce the friction coefficient and wear rate. These results reveal that the surface hardness of the U-rolled sample was higher than that of the T-rolled sample, whereas the milled sample showed the lowest surface hardness. Therefore, the friction and wear performance of the samples showed the following trend: U-rolled > T-rolled > milled.

4 Conclusions

(1) The surface roughness of the cladding layer processed by U-rolling was only 1/4 of that of the layer processed by T-rolling. The hardness and residual compressive stress of the laser cladding layer after U-rolling were higher than those after T-rolling. Compared to T-rolling, U-rolling exerts dynamic pressure on the surface, in addition to static pressure. Therefore, it produces a stronger surface hardening effect than T-rolling, which results in a large amplitude and depth of residual compressive stress.

(2) The self-corrosion potential of the U-rolled sample was higher than that of T-rolled, and the corrosion resistance of the U-rolled specimen was higher than that of T-rolled specimen. However, the corrosion current densities of the two were approximately equal, with a negligible difference in the corrosion rate. The curvature radius of the capacitive arc and the amplitudes in the medium- and low-frequency regions (10^{-2} < Frequency < 1) for the U-rolled

sample were larger than those for the T-rolled sample. The surface corrosion resistance of the laser cladding layer after U-rolling was higher than that after T-rolling. The effect of U-rolling on the corrosion resistance of the laser cladding layer is a result of the combined changes in the surface chemical and physical properties of the material (surface roughness, grain refinement, and residual compressive stress).

(3) The friction coefficient, wear pit width, depth, wear volume, and wear rate of the U-rolled surface of the cladding layer were lower than those of the T-rolled surface. Furthermore, the friction and wear performance of the U-rolled surface were found to be related to the rolling direction. When the surface friction direction was the same as the rolling direction, the friction and wear performance were higher than when the two directions were perpendicular. The U-rolled surface showed mainly abrasive and adhesive wear, whereas the T-rolled surface exhibited primarily adhesive wear.

Acknowledgements
Not applicable.

Author contributions
KZ and YL conceived and designed the experiments; JC and CL performed the rolling experiments; JC, CL and KZ analyzed the data; KZ, YL, JC and CL wrote the manuscript. All authors read and approved the final manuscript.

Authors' Information
Kaikui Zheng, born in 1986, is currently an associate professor and a master candidate supervisor at *School of Mechanical Engineering and Automation,* and *School of Advanced Manufacturing, Fuzhou University, China*. His main research interests include mechanical engineering, advanced manufacturing technology and tribology.
Youxi Lin, born in 1967, currently a professor and a PhD candidate supervisor at *School of Mechanical Engineering and Automation, Fuzhou University, China*. His main research interests include mechanical engineering and advanced manufacturing technology.
Jianguo Cai, born in 1989, is currently an engineer at *Mechanical and Electrical Engineering Practice Center, Fuzhou University, China*. He received his master degree on mechanical manufacturing and automation in *Fuzhou University, China*, in 2014.
Chengqian Lei, born in 1995, is currently a master candidate at *School of Mechanical Engineering and Automation, Fuzhou University, China*.

Funding
Supported by National Natural Science Foundation of China (Grant No. 51975123), Fujian Provincial Natural Science Foundation of China (Grant No. 2020J05115), Fuzhou Municipal Science and Technology Plan Project of China (Grant No. 2020-PT-148), and Quanzhou Municipal Science and Technology Plan Project of China (Grant No. 2020C043R).

Data Availability Statement
Authors can confirm that all relevant data are included in the article and/or its supplementary information files.

Competing interests
The authors declare no competing financial interests.

Author Details
[1]School of Mechanical Engineering and Automation, Fuzhou University, Fuzhou 350116, China. [2]School of Advanced Manufacturing, Fuzhou University, Jinjiang 362251, China. [3]Mechanical and Electrical Engineering Practice Center, Fuzhou University, Fuzhou 350116, China.

Received: 17 October 2021 Revised: 21 October 2022 Accepted: 26 October 2022
Published online: 18 November 2022

References

[1] T D Nguyen, P H Nguyen, L T Banh. Die steel surface layer quality improvement in titanium μ-powder mixed die sinking electrical discharge machining. *International Journal of Advanced Manufacturing Technology*, 2019, 100(9-12): 2637-2651.
[2] X Yang, C Li, Z Zhang, et al. Effect of cobalt-based coating microstructure on the thermal fatigue performance of AISI H13 hot work die steel. *Applied Surface Science*, 2020, 521: 146360.
[3] F Z Xuan, M L Zhu, G B Wang. Review and prospect of centennial research on structural fatigue. *Journal of Mechanical Engineering*, 2021, 57(6): 26-51. (in Chinese)
[4] A Lanzutti, M Pujatti, M Magnan, et al. Uniaxial fatigue properties of closed die hot forged 42CrMo4 steel: Effect of flash and mechanical surface treatments. *Materials & Design*, 2017, 132: 324-336.
[5] M Perini, P Bosetti. Die casting mold repair by hybrid manufacturing. *Journal of Materials Science and Engineering B*, 2019, 9(7-8): 144-152.
[6] L Shen, J Zhou, Y B Xiong, et al. Analysis of service condition of large hot forging die and refabrication of die by bimetal-layer weld surfacing technology with a cobalt-based superalloy and a ferrous alloy. *Journal of Manufacturing Processes*, 2018, 31: 731-743.
[7] H Y Wu, Y M Ye, H Q Lu, et al. Tribological behavior of laser thermal sprayed Cr3C2-NiCr + 10%Ni/MoS2 composite coating on H13 hot work mould steel. *Materials Research Express*, 2020, 7(1): 016599.
[8] D P Karmakar, G Muvvala, A K Nath. High-temperature abrasive wear characteristics of H13 steel modified by laser remelting and cladded with Stellite 6 and Stellite 6/30% WC. *Surface and Coatings Technology*, 2021, 422: 127498.
[9] J L Song, Y T Li, Q L Deng, et al. Research progress of laser cladding forming technology. *Journal of Mechanical Engineering*, 2010, 46(14): 29-39. (in Chinese)
[10] A A Siddiqui, A K Dubey. Recent trends in laser cladding and surface alloying. *Optics & Laser Technology*, 2021, 134: 106619.
[11] M S Xu, J F Li, H Lee, et al. Influence on powders and process parameters on bonding shear strength in laser cladding. *Journal of Mechanical Engineering*, 2017, 53(9): 209-216. (in Chinese)
[12] B S Xu, J X Fang, S Y Dong, et al. Heat-affected zone microstructure evolution and its effects on mechanical properties for laser cladding FV520B stainless steel. *Acta Metallurgica Sinica*, 2016, 52(1): 1-9. (in Chinese)
[13] S Y Dong, B S Xu, X B Liang, et al. Cracks in the laser cladded copper alloy coatings on aluminum alloy and its finite element analysis. *China Surface Engineering*, 2001, 14(4): 15-17. (in Chinese)
[14] Y H Zhao, J Sun, J F Li. Research on microstructure properties and wear and corrosion Resistance of FeCr repaired coating on KMN Steel by laser cladding. *Journal of Mechanical Engineering*, 2015, 51(8): 37-43. (in Chinese)
[15] T H N Pham, X W Zhang, C Q Wang, et al. Microstructure and mechanical properties of TiC /Co composite coating by laser cladding on H13 steel surface. *Transactions of the China Welding Institution*, 2013, 34(11): 27-31. (in Chinese)
[16] P Kattire, S Paul, R Singh, et al. Experimental characterization of laser cladding of CPM 9V on H13 tool steel for die repair applications. *Journal of Manufacturing Processes*, 2015, 20: 492-499.
[17] L Huang, J Z Zhou, J L Xu, et al. Microstructure and tribological properties of laser cladding NiCr/Cr3C2 coating on H13 steel surface. *Applied Laser*, 2019, 39(4): 556-562. (in Chinese)
[18] D L Cong , H Zhou, Z N Ren, et al. Thermal fatigue resistance of hot work die steel repaired by partial laser surface remelting and alloying process. *Optics & Lasers in Engineering*, 2014, 54(12): 55-61.

[19] Q L Dai, J Zhang, F Y You. Grinding characteristics of laser cladding Cr3C2/Ni based composite coating. *Journal of Harbin Institute of Technology*, 2019, 51(1): 122-126. (in Chinese)
[20] Q Y Wang, S L Bai, Y H Zhao, et al. Effect of mechanical polishing on corrosion behavior of Hastelloy C22 coating prepared by high power diode laser cladding. *Applied Surface Science*, 2014, 303: 312-318.
[21] T Roy, Q Lai, R Abrahams, et al. Effect of deposition material and heat treatment on wear and rolling contact fatigue of laser cladded rails. *Wear*, 2018, 412: 69-81.
[22] J Huang, K M Zhang, Y F Jia, et al. Effect of thermal annealing on the microstructure, mechanical properties and residual stress relaxation of pure titanium after deep rolling treatment. *Journal of Materials Science & Technology*, 2019, 35(3): 409-417.
[23] M L Zhu, J Long, F Z Xuan. Fatigue life and mechanistic modeling of interior micro-defect induced cracking in high cycle and very high cycle regimes. *Acta Materialia*, 2018, 157: 259-275.
[24] Y Meng, J X Deng, Y Zhang, et al. Tribological properties of textured surfaces fabricated on AISI 1045 steels by ultrasonic surface rolling under dry reciprocating sliding. *Wear*, 2020, 460: 203488.
[25] P R Zhang, Z Q Liu. Enhancing surface integrity and corrosion resistance of laser cladded Cr–Ni alloys by hard turning and low plasticity burnishing. *Applied Surface Science*, 2017, 409(1):169-178.
[26] W Zhuang, Q C Liu, R Djugum, et al. Deep surface rolling for fatigue life enhancement of laser clad aircraft aluminium alloy. *Applied Surface Science*, 2014, 320: 558-562.
[27] Z Q Liu, M He, J Zhao. Mechanical machining strengthening mechanism and material processing technology—a review. *China Mechanical Engineering*, 2015, 26(3): 403-413. (in Chinese)
[28] J X Zheng, Y L Guo, L X Zhu, et al. Cavitation effect in two-dimensional ultrasonic rolling process. *Ultrasonics*, 2021, 115: 106456.
[29] Q L Zhang, Z Q Hu, W W Su, et al. Microstructure and surface properties of 17-4PH stainless steel by ultrasonic surface rolling technology. *Surface and Coatings Technology*, 2017, 321: 64-73.
[30] H F Qin, Z C Ren, J Y Zhao, et al. Effects of ultrasonic nanocrystal surface modification on the wear and micropitting behavior of bearing steel in boundary lubricated steel-steel contacts. *Wear*, 2017, 392-393: 29-38.
[31] Y Liu, X H Zhao, D P Wang. Determination of the plastic properties of materials treated by ultrasonic surface rolling process through instrumented indentation. *Materials Science and Engineering: A*, 2014, 600(10): 21-31.
[32] A T Bozdana, N N Z Gindy, H Li. Deep cold rolling with ultrasonic vibrations—a new mechanical surface enhancement technique. *International Journal of Machine tools and manufacture*, 2005, 45(6): 713-718.
[33] M P Hu. *Corrosion electrochemistry*. Beijing: Metallurgical industry Press, 1991. (in Chinese)
[34] K K Zheng, Y X Lin, J G Cai, et al. Effect of ultrasonic rolling process on surface quality of laser cladding layer of die steel. *Journal of Mechanical Engineering*, 2022, 58(12): 111-120. (in Chinese)
[35] X Liu. *The surface rolling densification, friction and wear properties and rolling fatigue of the iron-based sintered material*. Guangzhou: South China University of Technology, 2016. (in Chinese)
[36] M J Yang. *Study on friction properties of ceramic powder/high density polyethylene composites*. Fuzhou: Fuzhou University, 2018. (in Chinese)